

## Simulation of decay processes and radiation transport times in radioactivity measurements



E. García-Toraño<sup>a,\*</sup>, V. Peyres<sup>a</sup>, M.-M. Bé<sup>b</sup>, C. Dulieu<sup>b</sup>, M.-C. Lépy<sup>b</sup>, F. Salvat<sup>c</sup>

<sup>a</sup> Laboratorio de Metrología de Radiaciones Ionizantes, CIEMAT, Avda. Complutense 22, 28040 Madrid, Spain

<sup>b</sup> CEA, LIST, Laboratoire National Henri Becquerel (LNE-LNHB), Bldg 602, PC111, 91191 Gif-sur-Yvette Cedex, France

<sup>c</sup> Facultat de Física (FQA and ICC), Universitat de Barcelona, Diagonal 647, 08028 Barcelona, Spain

### ARTICLE INFO

#### Article history:

Received 7 October 2016

Received in revised form 31 January 2017

Accepted 1 February 2017

Available online 20 February 2017

#### Keywords:

Nuclear decay

Radioactive sources

Monte Carlo radiation transport

Radiation detection

### ABSTRACT

The Fortran subroutine package PENNUC, which simulates random decay pathways of radioactive nuclides, is described. The decay scheme of the active nuclide is obtained from the NUCLEIDE database, whose web application has been complemented with the option of exporting nuclear decay data (possible nuclear transitions, branching ratios, type and energy of emitted particles) in a format that is readable by the simulation subroutines. In the case of beta emitters, the initial energy of the electron or positron is sampled from the theoretical Fermi spectrum. De-excitation of the atomic electron cloud following electron capture and internal conversion is described using transition probabilities from the LLNL Evaluated Atomic Data Library and empirical or calculated energies of released X rays and Auger electrons. The time evolution of radiation showers is determined by considering the lifetimes of nuclear and atomic levels, as well as radiation propagation times. Although PENNUC is designed to operate independently, here it is used in conjunction with the electron-photon transport code PENELOPE, and both together allow the simulation of experiments with radioactive sources in complex material structures consisting of homogeneous bodies limited by quadric surfaces. The reliability of these simulation tools is demonstrated through comparisons of simulated and measured energy spectra from radionuclides with complex multi-gamma spectra, nuclides with metastable levels in their decay pathways, nuclides with two daughters, and beta plus emitters.

© 2017 Elsevier B.V. All rights reserved.

### 1. Introduction

Practical situations involving radioactive sources are found in such diverse fields as nuclear spectroscopy, activity standardization, ionizing radiation metrology, radiation dosimetry, radiation protection, brachithery and nuclear medicine. Monte Carlo simulation methods are frequently used for quantitative studies in these fields, as well as for education and training. The simulation of experimental set-ups with radioisotopes that emit multiple photons and/or electrons of various energies, usually correlated in time, require specific procedures for sampling random decay pathways and accounting for the time evolution of particle histories. Even for nuclides with simple decay schemes, such as <sup>60</sup>Co, measured energy spectra may show sum peaks and other structures that result from time-correlated emissions. In addition, time correlations have a direct influence on coincidence measurements.

Modern Monte Carlo codes may offer the option of considering radioactive sources, either as a generic component of the original code or in the form of user-developed modules. Thus, Geant4<sup>1</sup> [1,2], includes a radioactive decay module based on data from the Evaluated Nuclear Structure Data File [3], which has been validated and refactored in [4,5]. To describe radioactive sources with codes where such a module is either unavailable or inconvenient, the user must define the decay scheme of the active nuclide and provide a dedicated subroutine that generates random decay pathways. The present article describes a systematic procedure for simulating the decay of radioactive nuclei, and its implementation within the Fortran Monte Carlo code PENELOPE [6], which performs simulations of coupled transport of photons and electrons (and positrons) in complex material structures consisting of homogeneous bodies limited by quadric surfaces [7–9]. The tools described here have evolved from previous works where the decay scheme of the active nuclide was defined manually [10]; and they are now tailored to facilitate simulations of nuclear spectroscopy measurements.

\* Corresponding author.

E-mail address: [e.garciatorano@ciemat.es](mailto:e.garciatorano@ciemat.es) (E. García-Toraño).

<sup>1</sup> Physics Reference Manual, version Geant4 10.3 (9 December, 2016).

We have written a Fortran subroutine package named `PENNUC` which simulates nuclear decay paths, and outputs the energies and directions of the emitted photons, electrons and positrons; alpha particles are not followed. These subroutines can be directly linked to the `PENELOPE` steering main program `penmain` and allow the simulation of experiments with radioactive sources containing a single active nuclide. Multiple radionuclides are not considered because results from measurements involving several nuclides can usually be modeled additively.

The decay scheme of the nuclide is obtained from the `NUCLEIDE` [11] database developed at the Laboratoire Nationale Henri Becquerel which includes data on 220 radioactive nuclides. The web application has been recently complemented with the option of exporting the nuclear decay characteristics (possible nuclear transitions, branching ratios, type and energy of emitted particles) in a text (ASCII) file with a format adapted to the `PENNUC` subroutines. These subroutines simulate the decay of the active nucleus as a random sequence of transitions; each transition involves either the release of electrons or photons with prescribed energies (beta and gamma transitions) or the production of a vacancy in an inner subshell of the active atom (internal conversion and electron capture). In the latter cases, subsequent relaxation of the atomic electron cloud is simulated by using transition probabilities and energies from the `PENELOPE` database [6]. The mean lifetimes of nuclear and electronic excited states are used to determine the emission time sequence. In spectroscopy simulations, excited levels with lifetimes longer than the resolution time of the detector, a parameter defined by the user, are considered as metastable levels. When the decay path includes a metastable level, the set of transitions prior to that level is considered as an independent emission event (in which several particles may be released). The emitted particles are fed to `PENELOPE`, which then simulates the coupled transport of photons and electrons (and positrons) in the material system. Optionally `PENELOPE` can keep track of the particle age (*i.e.*, the time elapsed since the start of the nuclear decay).

Although the `PENNUC` subroutines are tailored to be linked to `PENELOPE`, the package contains all necessary components (except the random number generator) to be used with any Monte Carlo radiation transport code. Thus, for the sake of portability, `PENNUC` contains a duplicate of the `PENELOPE` subroutines that describe the electronic de-excitation of atoms with vacancies in inner electron sub-shells. The `PENNUC` subroutines read relaxation parameters directly from a database file, which is part of the distribution package, and operate independently of their `PENELOPE` counterparts.

The present article is structured as follows. In Section 2 we briefly describe the models and methods implemented in the `PENNUC` subroutines for generating random nuclear decay pathways, including the sampling of the initial energy of beta particles as well as X rays and Auger electrons resulting from atomic de-excitation. Furthermore, the sampling of the lifetime of excited states and evaluation of the age of particles are described. In Section 3 we present comparisons of simulation results and measurements with various detectors of energy spectra from radioactive sources having non-trivial decay schemes. These comparisons evidence the reliability of the simulation models and code. Finally, concluding comments are provided in Section 4.

## 2. Methods

`PENNUC` delivers the initial-state variables of all particles released in the course of the decay process. These variables are: particle type (electron, photon, or positron), initial position coordinates ( $x, y, z$ ) (those of the active nucleus), direction cosines of the initial direction ( $u, v, w$ ), and energy (kinetic energy in the case of electrons and positrons). The position of the active nucleus is deter-

mined by `PENELOPE` according to the geometrical characteristics of the radioactive source. The initial direction of each particle is sampled randomly from the isotropic distribution, that is, possible angular correlations are disregarded. As already mentioned, in the case of alpha emitters, the alpha particle is not followed.

### 2.1. The `NUCLEIDE` database

As indicated above, the decay schemes of radionuclides are obtained from the `NUCLEIDE` database. This database contains evaluated data for about 220 radionuclides of practical interest in nuclear safety studies, environmental surveys, nuclear medicine, and a variety of other fields. The evaluation process is carried out within the framework of the Decay Data Evaluation Project (DDEP), an international cooperation project between different laboratories, which both discuss and agree on the evaluation methodology, and is coordinated by the Laboratoire National Henri Becquerel (LNHB). For each radionuclide, the evaluated data are determined from published experimental results and theoretical information, and they are accompanied with a detailed description of their evaluation and an exhaustive list of references. Evaluated nuclear and atomic decay data are then added to the `NUCLEIDE` database and are made available for further publication (web site, web application, printed report as Monographie BIPM-5 [12,13], data files, etc.). Finally, the recommended data, which are regularly updated, are presented in both a clear and easily readable form on the LNHB web site [11]. Recently, the option of downloading decay data in the `PENNUC` dedicated format has been made available on this site.

### 2.2. Sampling nuclear decay pathways from `NUCLEIDE` data

The type and energy of the particles released in each transition of the nucleus are determined randomly using the decay scheme and branching ratios provided by the `NUCLEIDE` database. As mentioned above, the processes of internal conversion and electron capture leave a vacancy in an inner electron sub-shell of the atom. The subsequent atomic relaxation is described by using the `PENELOPE` subroutine `relax` [6] (see Section 2.4).

To allow time correlations to be studied, we assign a certain resolution time to the detector, and consider all particles reaching the detector within this time as a single detection event. The lifetime  $t$  of a nuclear level with mean lifetime  $\tau$  is sampled from the familiar exponential distribution,

$$p(t) = \tau^{-1} \exp(-t\tau^{-1}). \quad (1)$$

In other words, we set

$$t = -\tau \ln \xi, \quad (2)$$

where  $\xi$  is a random number uniformly distributed in the interval (0,1). When the lifetime exceeds the detector resolution time, which is defined as a parameter in the Fortran source code, the level is considered as metastable. The set of consecutive transitions down to a metastable level, or to the ground level, is referred to as a “cascade”. In the evaluation of statistical uncertainties, a cascade is considered as a single emission event. Thus, the whole decay process to the final ground level of the daughter nucleus consists of either a single cascade or a sequence of cascades. In the latter case, each cascade may produce a separate “count” in the detector.

In `PENELOPE` the initial-state variables of the particles produced in the course of a shower are temporarily stored in a set of arrays called the secondary stack. The particles released in each cascade are sent to the secondary stack, except for the last one which is loaded in module `TRACK_mod` and considered as the “current” particle. The particles in the stack are tracked after completion of the current particle’s history.

### 2.3. Simulation of beta emission

Simulation of beta decays is based on analytical expressions of the energy spectra given in [14], which are derived from the formal theory of the process. The initial kinetic energy  $E$  of the electron or positron emitted in a beta transition is a random variable that takes values in the interval from zero up to a characteristic maximum energy  $E_m$ .

To simplify the analytical expressions, in this Section we use the natural system of units in which the reduced Planck's constant, the speed of light in vacuum and the electron mass are taken as unity ( $\hbar = c = m_e = 1$ ). The unit of energy is the electron rest energy  $m_e c^2 \simeq 511$  keV. The probability that a beta particle has initial kinetic energy between  $E$  and  $E + dE$  is given by

$$p_\beta(E) dE = C_\beta F_0(\zeta, E) L_0(\zeta, E) F_p(E, E_m) (E + 1)(E_m - E)^2 p dE, \quad (3)$$

where  $C_\beta$  is a normalization constant, and  $p$  is the linear momentum of the emitted particle,

$$p \equiv \sqrt{W^2 - 1}, \quad (4)$$

where  $W \equiv E + 1$  is the total energy, including the electron rest energy. The parameter  $\zeta$  is defined as  $\zeta = \alpha Z$  for  $\beta^-$  decay and  $\zeta = -\alpha Z$  for  $\beta^+$  decay where  $Z$  is the atomic number of the daughter nucleus and  $\alpha \simeq 1/137$  is the fine structure constant. The functions  $F_0$  and  $L_0$  are defined by the relations

$$F_0(\zeta, E) = 4(2pR)^{2g-2} \exp(-\pi y) \left| \frac{\Gamma(g + iy)}{\Gamma(2g + 1)} \right|^2 \quad (5)$$

and

$$L_0(\zeta, E) = 1 - \frac{7}{20} \zeta^2 - \frac{28}{15} WR\zeta - \frac{8}{15} \frac{R\zeta}{W} - \frac{1}{3} (pR)^2 - \frac{1}{5} \zeta^4 + \left(1 + \frac{9}{2} \zeta\right) (WR)^3 \zeta - \frac{1}{2} WR\zeta^3 + \frac{1}{20} \zeta^6 - \frac{3}{8} \zeta^8 - \frac{3}{8} WR\zeta^4 + 10(WR)^2 \zeta^6 \quad (6)$$

where

$$g \equiv \sqrt{1 - \zeta^2}, \quad y \equiv \zeta W/p_0, \quad (7)$$

and  $R$  is the nuclear radius, which is approximately given by

$$R = \frac{1}{386} \left(1.123A^{1/3} - 0.941A^{-1/3}\right) \quad (8)$$

where  $A$  stands for the mass number of the daughter nucleus. When  $E = 0$  the value of  $p_\beta(0)$  can be obtained from the relation

$$p_\beta(0) = C_\beta L_0(\zeta, 0) F_p(0, E_m) E_m^2 8\pi(2R\zeta)^{2g-2} \zeta |\Gamma(2g + 1)|^{-2}. \quad (9)$$

The shape of the spectrum depends on the type of transition through the prohibition factor  $F_p(E, E_m)$  in Eq. (3), which is determined by the parities and spins of the parent and daughter nuclei as shown in Table 1. Generic expressions for the prohibition factor are given in Table 1 in terms of the neutrino momentum

$$p_\nu \equiv E_m - E. \quad (10)$$

Empirical prohibition factors have been derived from measured energy spectra for those nuclides for which enough experimental information is available [15]. Our subroutines include these factors for a set of nuclides of metrological interest ( $^{11}\text{C}$ ,  $^{13}\text{N}$ ,  $^{18}\text{F}$ ,  $^{22}\text{Na}$ ,  $^{24}\text{Na}$ ,  $^{36}\text{Cl}$ ,  $^{32}\text{P}$ ,  $^{40}\text{K}$ ,  $^{49}\text{Sc}$ ,  $^{63}\text{Ni}$ ,  $^{68}\text{Ga}$ ,  $^{89}\text{Sr}$ ,  $^{90}\text{Sr}$ ,  $^{90}\text{Y}$ ,  $^{89}\text{Zr}$ ,  $^{99}\text{Tc}$ ,  $^{129}\text{I}$ ,  $^{138}\text{La}$ ,  $^{141}\text{Ce}$ ,  $^{186}\text{Re}$ ,  $^{204}\text{Tl}$ ,  $^{210}\text{Bi}$  and  $^{241}\text{Pu}$ ).

These analytical beta spectra are coded in the Fortran function `sbetas`, which is based on a program by Garcia-Toraño and Grau-Malonda [16]. The random sampling of the energy  $E$  of beta particles is performed by means of the RITA algorithm [6], which

**Table 1**

Classification of beta transitions according to spin and parity changes.  $J_p$  and  $J_d$  denote the spins of the parent and daughter nuclei, respectively. The last column gives the corresponding prohibition factors  $F_p(E, E_m)$  in Eq. (3). Empirical prohibition factors are also included in PENNUC for a number of selected radionuclides as explained in the text.

Kind of transition	$J_p - J_d$	Parity change	$F_p(E_0, E_m)$
Allowed	0, $\pm 1$	No	1
First forbidden	0, $\pm 1$	Yes	1
Unique first forbidden	$\pm 2$	Yes	$p^2 + p_\nu^2$
Second forbidden	$\pm 2$	No	$p^4 + p_\nu^2$
Unique second forbidden	$\pm 3$	No	$p^4 + p_\nu^4 + \frac{10}{3} p^2 p_\nu^2$
Third forbidden	$\pm 3$	Yes	$p^4 + p_\nu^4 + \frac{10}{3} p^2 p_\nu^2$
Unique third forbidden	$\pm 4$	Yes	$p^6 + p_\nu^6 + 7 p^2 p_\nu^2 (p^2 + p_\nu^2)$
Fourth forbidden	$\pm 4$	No	$p^6 + p_\nu^6 + 7 p^2 p_\nu^2 (p^2 + p_\nu^2)$

combines an adaptive rational interpolation of the inverse cumulative distribution function with an aliasing method [17]. The initial direction of the emitted particles is sampled isotropically. It is worth mentioning that the process of internal bremsstrahlung (i.e., the emission of a photon by the emitted beta particle in the screened field of the daughter atom) is not considered.

### 2.4. Generating atomic relaxation cascades

Radioactive nuclei are surrounded by the cloud of atomic electrons. The processes of electron capture and internal conversion remove one electron, preferentially from an inner (K or L) sub-shell, leaving the residual ion in a highly excited state. The ion subsequently relaxes to its ground state through a sequence of radiative and non-radiative transitions. In a radiative transition, the vacancy is filled by an electron from an outer sub-shell and an X ray with characteristic energy is emitted. In a non-radiative transition, the vacancy is filled by an outer electron and the excess energy is released through emission of an electron from a sub-shell that is further out (Auger effect). As in PENELOPE, we use the following notation to designate the possible transitions.

- Radiative: S0-S1 (an electron from the S1 shell fills the vacancy in the S0 shell, leaving a hole in the S1 shell).
- Non-radiative: S0-S1-S2 (an electron from the S1 shell fills the vacancy in the S0 shell, and the released energy is taken away by an electron in the S2 shell; this process leaves two vacancies in the S1 and S2 shells).

Atomic de-excitation cascades, with the associated emission of characteristic X rays and Auger electrons, are simulated by using the same method as in the subroutine `relax` of PENELOPE [6], a duplicate of which is included in the Fortran source file `pennuc.f`. Atomic relaxation data for each element are read from the file `pdrelax.pll` of the PENELOPE database, which contains a table of possible transitions, transition probabilities and energies of the emitted X rays or electrons for ionised atoms with a single vacancy in the K shell or in an L, M or N subshell. The transition probabilities were extracted from the LLNL Evaluated Atomic Data Library (EADL) [18]. The energies of X rays emitted in radiative transitions resulting from single vacancies in the K and L shells were taken from the compilation by Deslattes et al. [19]. X-ray energies for transitions of vacancies in M and N subshells were taken from Bearden's review and re-evaluation of experimental X-ray wavelengths [20].

In the case of radiative transitions S0-S1 not included in Bearden's tabulation, the energy of the X ray is taken from the EADL [18]. The energy of the electron emitted in a non-radiative transition S0-S1-S2 is also set equal to the EADL value. These transition

energies were estimated in terms of the energy eigenvalues of the DHFS self-consistent equations for neutral atoms in their ground states [18]. For tightly bound shells, with binding energies larger than about 200 eV, the DHFS energies agree closely with the ionisation energies recommended by Carlson [21,22].

The adopted energies for X rays and Auger electrons result from the approximation of assuming that the presence of the vacancy (or vacancies) does not alter the ionisation energies of the active electron shells. In addition, because these energies are also used for radiation emitted at any stage of the atomic de-excitation process, we are also neglecting changes in the emission energies caused by the possible relaxation of the ion [23]. Hence, our approach will not produce  $L_\alpha$  and  $L_\beta$  X-ray satellite lines; these arise from the filling of a vacancy in a doubly-ionised L shell, which releases energy that is slightly different from the energy emitted when the shell contains only a single vacancy. It is also worth recalling that the adopted transition probabilities are approximate. For K shells they are expected to be accurate to within about 1%, but for other shells they are subject to much larger uncertainties.

In the simulations, we set a suitable cut-off energy,  $E_c$ , and consider the shells with ionisation energies  $U_i$  larger than  $E_c$  as inner shells. Shells with ionisation energies less than  $E_c$ , or beyond the N7 shell, are regarded as outer shells.

Simulation of the relaxation cascade from a vacancy in an inner shell proceeds as follows. The transition that fills the initial vacancy is randomly selected according to the adopted transition probabilities by using Walker's aliasing method [6]. This transition leaves the ion with one or two vacancies. If the energy of the emitted characteristic X ray or Auger electron is larger than the corresponding absorption energy, the direction of emission is sampled from the isotropic distribution and the state variables of the particle are stored in the secondary stack. Generation of the cascade continues by repeating the process for each remaining vacancy. It ends when all inner subshells have been filled up.

It is important to bear in mind that transition probabilities from the EADL correspond to single vacancies. Additionally, we do not consider the relaxation of shells with principal quantum number larger than 4 (O, P, and Q subshells).

### 2.5. Radiation transport times

In experimental arrangements involving fast detection devices and/or coincidence techniques, the results of measurements may be affected by the time evolution of radiation showers. The time dependence of a shower can be described by attaching to each particle a state variable that measures the time elapsed since the start of the decay cascade. For brevity, we will refer to this time variable as the *age* of the particle.

Because the speed of photons with energies larger than about 100 eV in matter does not differ appreciably from the speed  $c$  of light in vacuum (see, e.g., Ref. [24]), the flight time of a photon between two events separated by a distance  $s$  is  $s/c$ .

While interaction events are assumed to occur instantaneously, the emission of X rays (and Auger electrons) after an ionisation event is delayed because of the finite lifetime of atomic energy levels [23]. The natural width  $\Gamma$  of an atomic energy level and the lifetime  $\tau$  of the states of that level are related by the time-energy uncertainty relation,

$$\Gamma\tau \simeq \hbar. \quad (11)$$

As noted by Richtmyer et al. [25], in the case of excitations which produce a single vacancy in an inner subshell, the first stage of subsequent decay of the ion is the filling of that vacancy by electrons from nearest shells, a process practically independent of the condition of the excited electron. Consequently, all excited levels with a vacancy in shell  $i$  have approximately the same level width,

$\Gamma_i$ , the so-called *core-level width*, and the same mean lifetime  $\tau_i = \hbar/\Gamma_i$ . Campbell and Papp [26] provide a set of recommended widths for K to N7 levels of atoms obtained from evaluation of available experimental data. For shells not included in these tables, we use calculated core-level widths given in the EADL [18]. Typically, the widths  $\Gamma_i$  increase with the binding energy of the shell; they are of the order of 0.1 eV or less for weakly bound shells, and reach values of the order of 100 eV for K shells of transuranic elements. The corresponding lifetimes have values of the order of  $10^{-14}$  to  $10^{-17}$  seconds.

Let us consider an atom with a vacancy in shell  $i$  at  $t = 0$ . The probability density function  $p(t)$  of the time  $t$  when the atom decays is the familiar exponential distribution with mean  $\tau_i$ ,

$$p(t) = \tau_i^{-1} \exp(-t\tau_i^{-1}). \quad (12)$$

We consider that the vacancy is filled after a random time  $t$  sampled from this distribution,

$$t = -\tau_i \ln \xi, \quad (13)$$

where  $\xi$  is a random number uniformly distributed in the interval (0,1). It is worth mentioning that we simulate relaxation cascades using atomic lifetimes that correspond to excited states with a single vacancy. To partially account for the possible occurrence of multiple vacancies, when in the course of a de-excitation cascade the active shell contains  $\nu > 1$  vacancies, their lifetime is set equal to  $\tau_i/\nu$ .

In PENELOPE electron and positron histories are described by using a class II scheme. In each trajectory segment between discrete events (hard interactions or hinges) the transported particle undergoes multiple soft inelastic collisions and soft bremsstrahlung emission events. The total energy loss  $W$  due to soft interactions along a segment of length  $s$  is a random variable with prescribed average value and variance. The effect of soft interactions is described as a continuous slowing down of the projectile with constant stopping power  $S_{\text{soft}} = W/s$ . Thus, the time spent by an electron with initial energy  $E_0$  to travel a trajectory segment of length  $s$  is given by

$$t(s) = \int_{E_0 - S_{\text{soft}}s}^{E_0} \frac{1}{\nu(E) S_{\text{soft}}} dE,$$

where

$$\nu(E) = c \frac{\sqrt{E(E + 2m_e c^2)}}{E + m_e c^2}$$

is the relativistic velocity of an electron with energy  $E$ . The integral is elementary,

$$t = \frac{1}{cS_{\text{soft}}} \left[ \sqrt{E(E + 2m_e c^2)} - \sqrt{(E - S_{\text{soft}}s)(E - S_{\text{soft}}s + 2m_e c^2)} \right]. \quad (14)$$

This formula is utilised in the simulation program for on-the-fly calculation of the age of electrons and positrons.

### 3. Miscellaneous applications

To illustrate the capabilities of PENNOC we present here examples of simulations of measurements and applications that involve non-trivial situations. These include multi-gamma emitting radionuclides, nuclides with metastable levels in their decay pathways, nuclides with two daughters, and beta plus emitters.

All measurements presented below were performed with HPGe detectors with enhanced low-energy detection capabilities surrounded by lead shields to reduce the radiation background, and with point or volume radioactive sources. The geometrical details

of the experimental set-ups were described by means of the `PENGEOM` package [27]. The example shown in Fig. 1 corresponds to an HPGe portable [28] detector with a volume source of  $^{192}\text{Ir}$  placed at a short distance from the detector window.

Simulated energy spectra are usually generated by scoring the total energy deposited within the active volume of the detector by the particles in each cascade. Thus, sum peaks and escape peaks are consistently described by the simulation code. The deposited energy spectrum resulting from a simulation is in the form of a histogram,  $P_{\text{MC}}(E)$ , with a certain bin width  $\Delta$ . Because radiations emitted by the active nuclide, and during atomic relaxation, have well-defined energies, each line is fully contained in a single channel of the output histogram. To compare with measured spectra we must account for fluctuations in the electronic amplification of output pulses, and other effects, which determine the energy resolution of the detector [29]. For this purpose, we consider the energy-resolution function  $R_d(E, E_{\text{ch}})$  defined as the probability (normalized to unity) that a deposited energy  $E$  produces a count in the energy channel corresponding to energy  $E_{\text{ch}}$ . For many detectors, the energy resolution function can be approximated as a Gaussian,

$$R_d(E, E_{\text{ch}}) = \frac{1}{\sqrt{2\pi}\sigma(E)} \exp\left[-\frac{1}{2}\left(\frac{E - E_{\text{ch}}}{\sigma(E)}\right)^2\right], \quad (15)$$

with

$$\sigma(E) = \frac{1}{\sqrt{8 \ln 2}} \Gamma_d(E). \quad (16)$$

where  $\Gamma_d(E)$  is the full-width-at-half-maximum of a spectral line centered at the energy channel  $E$ .

Given a calculated energy-deposition spectrum  $P_{\text{MC}}(E)$ , we calculate the corresponding “simulated” spectrum  $P(E)$  as the convolution of  $P_{\text{MC}}(E)$  with the energy-resolution function of the detector. That is,

$$P(E_{\text{ch}}) = \int_0^\infty [P_{\text{MC}}(E)\epsilon_d(E)]R_d(E, E_{\text{ch}})dE. \quad (17)$$

It is worth noting that this formula is valid only if the bin width  $\Delta$  of the simulated histogram is much smaller than the energy resolution  $\Gamma_d(E)$ . When this is not the case,  $\Gamma_d(E)$  should be replaced by  $\Gamma_d(E) - \Delta$ . The simulated spectra presented below have been calculated by transforming the energy-deposition spectra according to Eq. (17), with the  $\Gamma_d(E)$  function determined empirically for each detector.

### 3.1. Multi-gamma-emitting radionuclides

In measurements of energy spectra of radionuclides whose decay scheme include a large number of gamma transitions, the effect of summing-in or summing-out processes associated with coincidence-summing is difficult to calculate by analytical correction methods. In contrast, Monte Carlo simulation of the decay process provides a convenient solution and yields reliable estimates of summing corrections. As an extreme example, we consider the nuclide  $^{166\text{m}}\text{Ho}$  which decays to  $^{166}\text{Er}$  via several beta transitions [12], and releases a large number of gamma-rays in the subsequent de-excitation of the excited levels of  $^{166}\text{Er}$ . In 2013, a EURAMET comparison of activity concentration measurements of the same solution of this nuclide, was carried out with the participation of six European laboratories [30]. The `PENNUC` routines were used at CIEMAT for two aims: 1) to simulate the gamma spectra measured with a HPGe detector, and 2) to calculate the counting efficiency required by one of the calibration methods used in the exercise, the so-called  $4\pi\gamma$  or integral gamma counting for which, a well-type scintillation counter was used. Fig. 2 compares experimental

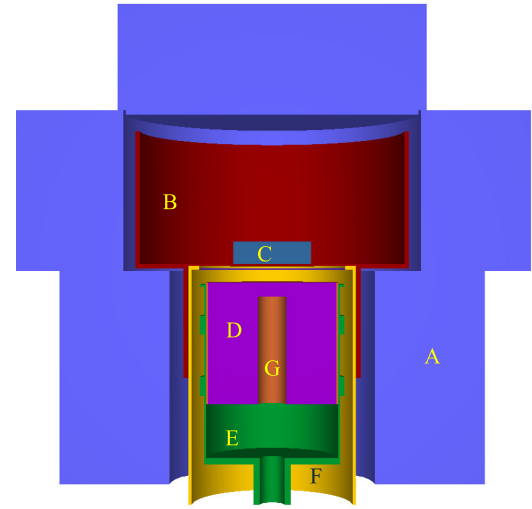


**Fig. 1.** Geometrical model of a measurement setup used in the present simulations, as displayed by the `PENGEOM` 3D viewer. A volume source of stainless steel contaminated with  $^{192}\text{Ir}$  is placed in a thin-wall plastic chamber in contact with the detector window. A: Lead shield, B: Measurement chamber, C: Radioactive source, D: Active Ge, E: Crystal holder, F: End cup, G: Core hole.

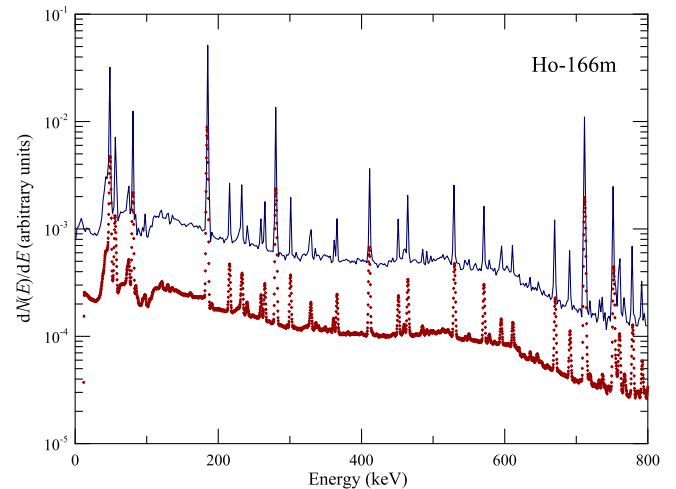


**Fig. 2.** Simulated (upper) and measured (lower) spectra of a volume source of  $^{166\text{m}}\text{Ho}$  measured with an HPGe detector.

and simulated spectra taken with an extended-range HPGe detector in the energy range up to 800 keV. The agreement between simulated and measured spectra is excellent, particularly regarding the sum peaks originated in the photon cascades. The correctness of the algorithm was further confirmed by the results obtained in the calibration using the  $4\pi\gamma$  technique in the above-mentioned international comparison [30].

Coincidence-summing with X rays following atomic rearrangement can always affect the measurement by gamma spectrometry, but is especially significant for nuclides that decay by electron-capture. One of the most relevant examples is  $^{133}\text{Ba}$ , which decays to  $^{133}\text{Cs}$  through 5 electron-capture branches, and many coincidence-summing events occur between the X rays that follow the electron capture and the gamma rays that depopulate the excited levels [13] of  $^{133}\text{Cs}$ . Its decay scheme is depicted in Fig. 3. Fig. 4 presents a region of the gamma spectrum of this nuclide which shows several structures that can be assigned to X ray-gamma coincidences. The result of the simulation, also shown in the figure, closely reproduces the experimental data. The degree

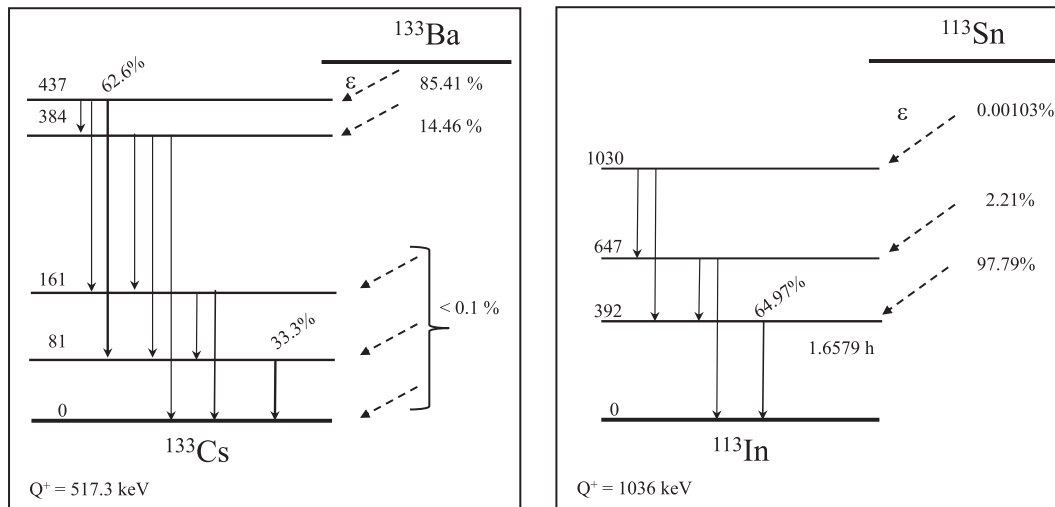


Fig. 3. Simplified decay scheme of the nuclides  $^{133}\text{Ba}$  and  $^{113}\text{Sn}$ . Data taken from Refs. [13,12].

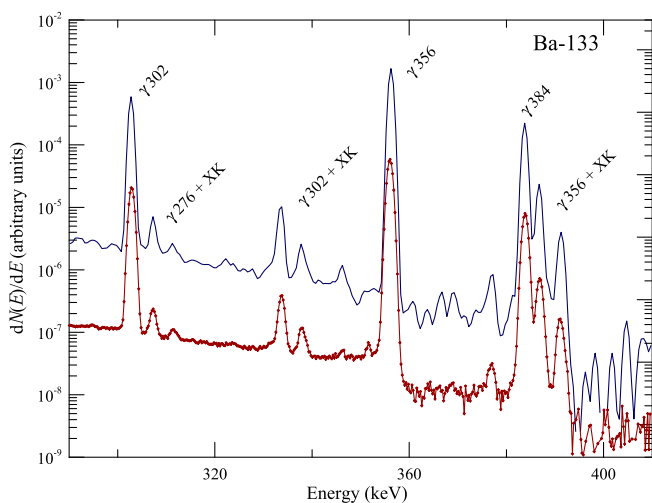


Fig. 4. Simulated (upper) and measured (lower) spectra of a point source of  $^{133}\text{Ba}$  measured with an HPGe detector. The energy interval from 290 keV to 410 keV displayed here contains strong coincidence summing with X ray lines.

of agreement between simulation and experiment has been quantified by considering the efficiencies determined by numerical analysis of peak areas; the differences between measured and calculated efficiencies for the gamma transitions of 80.89, 276.4, 356.01, and 383.85 keV are less than 1 %.

A further example of complex spectra is provided by the nuclide  $^{192}\text{Ir}$ , which decays to two daughters: by beta minus emission to  $^{192}\text{Pt}$ , and by electron capture to  $^{192}\text{Os}$  [12]. A volume source of this nuclide (a stainless steel contaminated disk) was standardized by  $\gamma$  spectrometry, using the set-up presented in Fig. 1, within the framework of a recent European Research Metrology Project [31]. For volume sources, coincidence-summing corrections are difficult to calculate because the efficiency, and therefore the corrections, have to be calculated by taking into account the location of the emitting nucleus, which determines the absorption of radiation within the source. Results have proved that the algorithm provides an accurate estimation of this effect [31].

### 3.2. Nuclides with metastable energy levels

For radionuclides whose decay schemes include metastable levels, time coincidences between events have to be calculated

by taking into account the time  $t$  the nucleus spends in the metastable level, which is sampled from the exponential distribution with mean equal to the level lifetime (see Section 2.2). One of such nuclides is  $^{113}\text{Sn}$  which has the relatively simple decay scheme displayed in Fig. 3 [12]. It disintegrates to  $^{113}\text{In}$ , mainly by electron capture (97.79%) to the metastable 392 keV level and partially by electron capture (2.21%) to the 647 keV excited level, [12]. Consequently, the complete decay includes both prompt transitions and transitions that start at the metastable level. Activity standardization of this nuclide must then account for both contributions, as explained in Ref. [32], which describes the standardization by three techniques, two of which ( $4\pi\gamma$  counting and Liquid Scintillation Counting) required the use of the Monte Carlo simulation techniques described in the present article. Results obtained by the three techniques are in excellent agreement [32].

### 3.3. Positron-emitting nuclides

Positron emitting nuclides are of particular interest because of their potential applications in nuclear medicine. For instance,  $^{44}\text{Sc}$  is used as a long-lived PET radionuclide and, combined with its isotope  $^{47}\text{Sc}$ , a beta minus emitter, is considered as a promising *theranostic* alternative in nuclear medicine [33]. The  $^{44}\text{Sc}$  nucleus

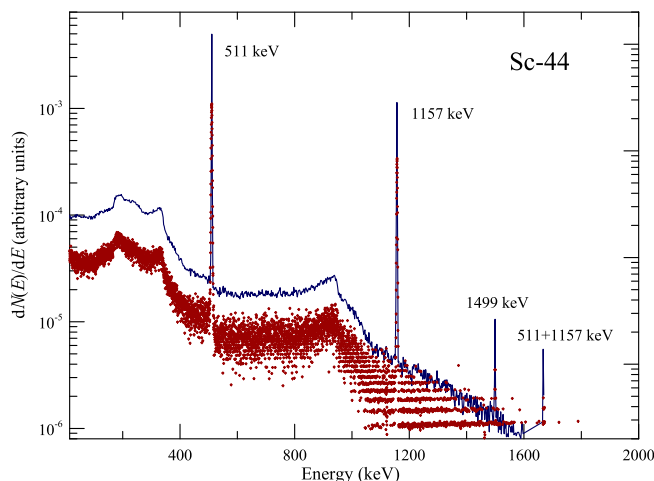


Fig. 5. Simulated (upper) and measured (lower) spectra of a point source of the positron emitter nuclide  $^{44}\text{Sc}$ , measured with an HPGe detector.

disintegrates by beta plus emission (94.27%) and by electron capture (5.73%) to  $^{44}\text{Ca}$ . Most decays (99%) feed an excited level of the daughter nucleus which de-excites to the ground level by emission of a gamma ray of 1157 keV [12]. Simulated and measured spectra from a  $^{44}\text{Sc}$  source recorded with an HPGe detector are shown in Fig. 5, where the structures corresponding to the 511 keV annihilation peak and the 1157 keV gamma emission are prominent; their sum peak is also visible at the upper end of the spectrum. The low energy region of the spectrum (with the backscattering contribution and the Compton edge) is also well reproduced by the simulation [34].

#### 4. Concluding comments

We have described the subroutine package PENNNUC for simulation of the decay pathways of radioactive sources containing a single active nuclide. The PENNUC subroutines linked to the Monte Carlo code PENELOPE allow the simulation of measurements and applications involving radioactive sources in complex material structures. The combined simulation code has been shown to yield results in good agreement with metrology measurements involving nuclides having complex spectra, nuclides with metastable states, nuclides with two daughters, and positron emitters.

Although the current PENNUC subroutines are tailored to work with PENELOPE, they are flexible enough to be used in any Monte Carlo simulation code. The subroutine package and the associated data files, accompanied with documented examples, will be made available in due course.

#### Acknowledgements

We are thankful to F. Salvat-Pujol for critically reading the manuscript. FS gratefully acknowledges financial support from the Spanish Ministerio de Economía y Competitividad and ERDF (project No. FPA2013-44549-P) and from the Generalitat de Catalunya, Spain (grant 2014 SGR 846).

#### References

- [1] S. Agostinelli, J. Allison, K. Amako, J. Apostolakis, H. Araujo, P. Arce, M. Asai, Geant4—a simulation toolkit, *Nucl. Instrum. Meth. A* 506 (2003) 250–303.
- [2] J. Allison, K. Amako, J. Apostolakis, H. Araujo, P. Arce Dubois, M. Asai, Geant4 developments and applications, *IEEE Trans. Nucl. Sci.* 53 (2006) 270–278.
- [3] J. Tuli, Evaluated nuclear structure data file, *Nucl. Instrum. Methods Phys. Res., Sect. A* 369 (2–3) (1996) 506–510, Available from <http://www.nndc.bnl.gov/ensdf/>.
- [4] S. Hauf, M. Kuster, M. Batič, Z.W. Bell, D.H.H. Hoffmann, P.M. Lang, S. Neff, M.G. Pia, G. Weidenspointner, A. Zoglauer, Validation of Geant4-based radioactive decay simulation, *IEEE Trans. Nucl. Sci.* 60 (4) (2013) 2984–2997.
- [5] S. Hauf, M. Kuster, M. Batič, Z.W. Bell, D.H.H. Hoffmann, P.M. Lang, S. Neff, M.G. Pia, G. Weidenspointner, A. Zoglauer, Radioactive decays in Geant 4, *IEEE Trans. Nucl. Sci.* 60 (4) (2013) 2966–2983.
- [6] F. Salvat, penelope-2014: A code System for Monte Carlo Simulation of Electron and Photon Transport, OECD/NEA Data Bank, NEA/NSC/DOC(2015) 3, Issy-les-Moulineaux, France, 2015. Available from <http://www.nea.fr/lists/penelope.html>.
- [7] J. Baró, J. Sempau, J.M. Fernández-Varea, F. Salvat, PENELOPE: an algorithm for Monte Carlo simulation of the penetration and energy loss of electrons and positrons in matter, *Nucl. Instrum. Meth. B* 100 (1995) 31–46.
- [8] E. Benedetto, J.M. Fernández-Varea, F. Salvat, Mixed simulation of the multiple elastic scattering of electrons and positrons using partial-wave differential cross sections, *Nucl. Instrum. Meth. B* 174 (2001) 91–110.
- [9] J. Sempau, J.M. Fernández-Varea, E. Acosta, F. Salvat, Experimental benchmarks of the Monte Carlo code PENELOPE, *Nucl. Instrum. Meth. B* 207 (2003) 107–123.
- [10] E. García-Toraño, M. Pozuelo, F. Salvat, Monte Carlo calculations of coincidence-summing corrections for volume sources in gamma-ray spectrometry with Ge detectors, *Nucl. Instrum. Meth. Phys. Res., Sect. A* 544 (3) (2005) 577–583.
- [11] <http://www.nucleide.org/DDEPWWG/DDEPdata.htm>. Last accessed December 16, 2016
- [12] M.-M. Bé, V. Chisté, C. Dulieu, E. Browne, V. Chechev, N. Kuzmenko, R. Helmer, A. Nichols, E. Schönfeld, R. Dersch, Table of Radionuclides, Vol. 1 of Monographie BIPM-5, Bureau International des Poids et Mesures, Pavillon de Breteuil, F-92310 Sèvres, France, 2004.
- [13] M.-M. Bé, V. Chisté, C. Dulieu, E. Browne, C. Baglin, V. Chechev, N. Kuzmenko, R. Helmer, F. Kondev, D. MacMahon, K. Lee, Monographie BIPM-5, Table of Radionuclides, Vol. 3 ISBN 92-822-2218-7, Vol. 3 of Monographie BIPM-5, Bureau International des Poids et Mesures, Pavillon de Breteuil, F-92310 Sèvres, France, 2006.
- [14] A. Grau-Malonda, E. García-Toraño, Evaluation of counting efficiency in liquid scintillation counting of pure  $\beta$ -ray emitters, *Int. J. Appl. Radiat. Isot.* 33 (4) (1982) 249–253.
- [15] X. Mougeot, Reliability of usual assumptions in the calculation of  $\beta$  and  $\nu$  spectra, *Phys. Rev. C* 91 (2015) 055504.
- [16] E. García-Toraño, A. Grau-Malonda, EFFY, a new program to compute the counting efficiency of beta particles in liquid scintillators, *Comput. Phys. Commun.* 36 (1985) 307–312.
- [17] A.J. Walker, An efficient method for generating discrete random variables with general distributions, *ACM Trans. Math. Software* 3 (1977) 253–256.
- [18] S.T. Perkins, D.E. Cullen, M.H. Chen, J.H. Hubbell, J. Rathkopf, J. Scofield, Tables and graphs of atomic subshell and relaxation data derived from the LLNL evaluated atomic data library (EADL),  $Z = 1-100$ , Tech. Rep. UCLL-ID-50400, Lawrence Livermore National Laboratory, Livermore, California, 1991.
- [19] R.D. Deslattes, E.G. Kessler, P. Indelicato, L. de Billy, E. Lindroth, J. Anton, X-ray transition energies: new approach to a comprehensive evaluation, *Rev. Mod. Phys.* 75 (2003) 36–99.
- [20] J.A. Bearden, X-ray wavelengths, *Rev. Mod. Phys.* 39 (1967) 78–124.
- [21] T.A. Carlson, Photoelectron and Auger Spectroscopy, Plenum Press, New York, 1975.
- [22] F. Salvat, J.M. Fernández-Varea, Overview of physical interaction models for photon and electron transport used in Monte Carlo codes, *Metrologia* 46 (2009) S112–S138.
- [23] K.D. Sevier, Low Energy Electron Spectrometry, Wiley Interscience, New York, 1972.
- [24] E.D. Palik (Ed.), Handbook of Optical Constants of Solids, Academic Press, San Diego, CA, 1985.
- [25] F.K. Richtmyer, S.W. Barnes, E. Ramberg, The widths of the L-series lines and of the energy levels of Au(79), *Phys. Rev.* 15 (1934) 843–860.
- [26] J.L. Campbell, T. Papp, Widths of the atomic K-N7 levels, *At. Data Nucl. Data Tables* 77 (2001) 1–56.
- [27] J. Almansa, F. Salvat-Pujol, G. Díaz-Londoño, A. Carnicer, A.M. Lallena, F. Salvat, PENGEO – a general-purpose geometry package for Monte Carlo simulation of radiation transport in material systems defined by quadric surfaces, *Comput. Phys. Commun.* 199 (2016) 102–113.
- [28] V. Peyres, E. García-Toraño, Efficiency calibration of an extended-range Ge detector by a detailed Monte Carlo simulation, *Nucl. Instrum. Meth. Phys. Res., Sect. A* 580 (2007) 296–298, Proceedings of the 10th International Symposium on Radiation Physics ISRP 10.
- [29] J. Šolc, P. Dryák, H. Moser, T. Branger, E. García-Toraño, V. Peyres, F. Tzika, G. Lutter, M. Capogni, A. Fazio, A. Luca, B. Vodenik, C. Oliveira, A. Saraiva, L. Szucs, T. Dziel, O. Burda, D. Arnold, J. Martinković, T. Siiskonen, A. Mattila, Characterisation of a radionuclide specific laboratory detector system for the metallurgical industry by monte carlo simulations, *Radiat. Phys. Chem.* 116 (2015) 189–193, Proceedings of the 9th International Topical Meeting on Industrial Radiation and Radioisotope Measurement Applications.
- [30] K. Kossert, T. Altitzoglou, P. Auerbach, M.-M. Bé, C. Bobin, P. Cassette, E. García-Toraño, H. Grigaut-Desbrosses, H. Isnard, V. Lourenço, O. Nähle, J. Paepen, V. Peyrés, S. Pommé, A. Rozkov, A.I. Sanchez-Cabezudo, J. Sochorová, C. Thiam, R.V. Ammel, Results of the EURAMET.RI(II)-K2.Ho-166m activity comparison, *Metrologia* 51 (1A) (2014) 06022.
- [31] A. Petrucci, D. Arnold, O. Burda, P. De Felice, E. García-Toraño, M. Mejuto, V. Peyres, J. Šolc, B. Vodenik, Evaluation of HPGe spectrometric devices in monitoring the level of radioactive contamination in metallurgical industry, *Nucl. Instrum. Meth. Phys. Res. A* 797 (2015) 271–277.
- [32] M. Roteta, V. Peyres, E. García-Toraño, Standardization of Sn-113, *Appl. Radiat. Isot.* 87 (2014) 162–165.
- [33] F. Rosch, R.P. Baum, Generator-based PET radiopharmaceuticals for molecular imaging of tumours: on the way to THERANOSTICS, *Dalton Trans.* 40 (2011) 6104–6111.
- [34] E. García-Toraño, V. Peyres, M. Roteta, A.I. Sánchez-Cabezudo, E. Romero, A. Martínez Ortega, Standardisation and precise determination of the half-life of  $^{44}\text{Sc}$ , *Appl. Radiat. Isot.* 109 (2016) 314–318, Proceedings of the 20th International Conference on Radionuclide Metrology and its Applications 8–11 June 2015, Vienna, Austria.